Author Manuscript

Author Manuscript

Author Manuscript

Author Manuscript

HHS Public Access

Author manuscript

Nanotoxicology. Author manuscript; available in PMC 2017 August 01.

Published in final edited form as:

Nanotoxicology. 2016 August ; 10(6): 720–727. doi:10.3109/17435390.2015.1113322.

Surface modification of zinc oxide nanoparticles with amorphous silica alters their fate in the circulation

Nagarjun V. Konduru, **Kimberly M. Murdaugh**, **Archana Swami**, **Renato Jimenez**, **Thomas C. Donaghey**, **Philip Demokritou**, **Joseph D. Brain**, and **Ramon M. Molina***

Molecular and Integrative Physiological Sciences Program and Center for Nanotechnology and Nanotoxicology, Department of Environmental Health, Harvard T.H. Chan School of Public Health, 665 Huntington Avenue, Boston, MA 02115, USA

Abstract

Nanoparticle (NP) pharmacokinetics and biological effects are influenced by many factors, especially surface physicochemical properties. We assessed the effects of an amorphous silica coating on the fate of zinc after intravenous (IV) injection of neutron activated uncoated ^{65}ZnO or silica-coated ^{65}ZnO NPs in male Wistar Han rats. Groups of IV-injected rats were sequentially euthanized, and 18 tissues were collected and analyzed for ^{65}Zn radioactivity. The protein coronas on each ZnO NP after incubation in rat plasma were analyzed by SDS-PAGE gel electrophoresis and mass spectrometry of selected gel bands. Plasma clearance for both NPs was biphasic with rapid initial and slower terminal clearance rates. Half-lives of plasma clearance of silica-coated ^{65}ZnO were shorter (initial - <1 minute; terminal - 2.5 minutes) than uncoated ^{65}ZnO (initial - 1.9 minutes; terminal - 38 minutes). Interestingly, the silica-coated ^{65}ZnO group had higher ^{65}Zn associated with red blood cells and higher initial uptake in the liver. The ^{65}Zn concentrations in all the other tissues were significantly lower in the silica-coated than uncoated groups. We also found that the protein corona formed on silica-coated ZnO NPs had higher amounts of plasma proteins, particularly albumin, transferrin, A1 inhibitor 3, α-2-hs-glycoprotein, apoprotein E, and α-1 antitrypsin. Surface modification with amorphous silica alters the protein corona, agglomerate size, and zeta potential of ZnO NPs, which in turn influences ZnO biokinetic behavior in the circulation. This emphasizes the critical role of the protein corona in the biokinetics, toxicology, and nanomedical applications of nanoparticles.

Keywords

silica coating; nanoparticles; biokinetics; surface chemistry; zinc radioisotope

*Corresponding Author: Ramon M. Molina, Molecular and Integrative Physiological Sciences Program, Department of Environmental Health, Harvard T.H. Chan School of Public Health, 665 Huntington Avenue, Boston, MA 02115, USA, Phone: 1-617-432-2311, Fax: 1-617-432-4710, rmolina@hsph.harvard.edu.

Competing interests

The authors declare no competing interests.

Author Manuscript Author Manuscript Author Manuscript Author Manuscript

INTRODUCTION

Zinc oxide (ZnO) is a widely used additive in ceramics, plastics, cement, sealants, foods, and cosmetics. In addition, semiconducting and optical properties make it useful for a variety of technological applications, ranging from sensors, light emitting diodes, and solar cells (Djurisic and Leung, 2006, Su et al., 2010). In recent years, there has been an increase in the production of ZnO nanoparticles (NPs) resulting from development of more sophisticated techniques in nanotechnology and novel synthetic methods. ZnO NPs have unique properties that are different from larger ZnO particles, including increased reactivity and enhanced UV filtering ability (Baek et al., 2012, Baek et al., 2011). ZnO NPs are commonly added to sunscreens because of their ability to absorb both UV-A and UV-B radiation (Nohynek et al., 2008, Nohynek et al., 2007). Despite the widespread advantages of ZnO NPs, their use is sometimes limited due to potential toxicity. ZnO NPs undergo dissolution releasing Zn^{2+} ions responsible for their cytotoxic effects (Alarifi et al., 2013, De Berardis et al., 2010, Warheit et al., 2009, Xia et al., 2008). In general, the particle solubility increases as the nanoparticle size decreases (Kreyling et al., 1990) (Baek et al., 2011). This increases concerns regarding nanoparticles' health effects.

A safer formulation concept for the synthesis of metal oxide NPs has been proposed (Demokritou et al., 2013, Gass et al., 2013, Sotiriou et al., 2014). This method employs flame spray pyrolysis using the Versatile Engineered Nanomaterial Generation System (VENGES) to coat the nanoparticles with a thin layer of amorphous silica. It has been shown that silica coating mitigates ZnO nanoparticle toxicity and potential for DNA damage in vitro (Sotiriou et al., 2014). The protective effects of silica coating observed in this study were correlated with decreased in vitro dissolution of ZnO in cell-free culture media.

The biokinetic behavior of NPs is influenced by surface characteristics of NPs, such as their chemical and molecular structure (Choi et al., 2007, Choi and Choy, 2014, Konduru et al., 2015, Moghimi et al., 2012, Shim et al., 2014). Surface chemistry influences the adsorption of plasma lipids, proteins and other components of blood in the formation of a particle corona, which may regulate the overall nanoparticle pharmacokinetics and biological responses (Konduru et al., 2015, Kreyling et al., 2014). Pharmacokinetic studies using neutron activated uncoated ZnO NPs have been published previously (Yeh et al., 2012, Choi and Choy, 2014, Chen et al., 2010, Konduru et al., 2014, Paek et al., 2013). These studies explored the role of primary NP size on biokinetics of IV-injected (Yeh et al., 2012), orally administered (Baek et al., 2012) (Konduru et al., 2014) and intratracheally instilled ZnO NPs (Konduru et al., 2014). We have also studied the role of silica coating on biokinetics of IT-instilled and gavaged ZnO NPs (Konduru et al., 2014). However, the effects of the silica coating on the pharmacokinetics of IV-injected ^{65}ZnO have not been explored. Here, we present a pharmacokinetic study of IV-injected ^{65}ZnO and silica-coated ^{65}ZnO NPs over a period of 7 days in male Wistar Han rats.

Author Manuscript Author Manuscript Author Manuscript Author Manuscript

Methods

Synthesis of uncoated ZnO and silica-coated ZnO nanoparticles

The synthesis of these NPs was reported previously (Sotiriou et al., 2014). In brief, uncoated and silica-coated ZnO particles were synthesized by flame spray pyrolysis (FSP) of zinc naphthenate (Sigma-Aldrich, St. Louis, MO, USA) dissolved in ethanol (Sigma-Aldrich) at a precursor molarity of 0.5 M. The precursor solution was fed through a stainless steel capillary at 5 ml/min, dispersed by 5 L/min O_2 (purity >99%, pressure drop at nozzle tip: p_{drop} = 2 bar) (Air Gas, Berwyn, PA, USA) and combusted. A premixed methane-oxygen (1.5 L/min, 3.2 L/min) supporting flame was used to ignite the spray. Oxygen sheath gas was used at 40 L/min. Core particles were coated in flight by the swirl-injection of hexamethyldisiloxane (HMDSO) (Sigma Aldrich, St. Louis, MO, USA) through a torus ring with 16 jets at an injection height of 200 mm above the FSP burner. A total gas flow of 16 L/min, consisting of N_2 carrying HMDSO vapor and pure N_2, was injected through the torus ring jets. HMDSO vapor was obtained by bubbling N_2 gas through liquid HMDSO (500 ml) maintained at constant temperature using a temperature-controlled water bath.

Characterization of uncoated ZnO and silica-coated ZnO nanoparticles

The synthesis and characterization of these NPs were reported previously (Konduru et al., 2014, Sotiriou et al., 2014). Their morphology was examined by transmission electron microscopy (TEM). Uncoated and silica-coated ZnO NPs were dispersed in ethanol at a concentration of 1 mg/ml in 50 ml polyethylene conical tubes and sonicated at 246 J/ml (Branson Sonifier S-450A, Swedesboro, NJ, USA). The samples were deposited onto lacey carbon TEM grids. All grids were imaged with a JEOL 2100 (JEOL USA, Inc., Peabody, MA, USA). The primary particle size was determined by X-ray diffraction (XRD). XRD patterns for uncoated ZnO and silica-coated ZnO NPs were obtained using a Scintag XDS2000 powder diffractometer (Cu Kα, λ = 0.154 nm, 40 kV, 40 mA, stepsize = 0.02°). One hundred milligrams of each sample was placed onto the diffractometer stage and analyzed from a range of 2θ = 20–70°. Major diffraction peaks were identified using the Inorganic Crystal Structure Database (ICSD) for wurtzite (ZnO) crystals. The crystal size was determined by applying the Debye-Scherrer Shape Equation to the Gaussian fit of the major diffraction peak. The specific surface area was obtained using the Brunauer-Emmet-Teller (BET) method. The samples were degassed in N_2 for at least 1 hour at 150°C before obtaining five-point N_2 adsorption at 77 K (Micrometrics Tristar 3000, Norcross, GA, USA).

Neutron activation of nanoparticles

Both coated and uncoated ZnO nanoparticles were neutron-activated at the Massachusetts Institute of Technology (MIT) Nuclear Reactor Laboratory (Cambridge, MA, USA). Samples were irradiated with a thermal neutron flux of 5×10^{13} n/cm^{2}s for 120 hours. The resulting ^{65}Zn radioisotope has a half-life of 244.3 days and a primary gamma energy peak of 1115 keV. The specific activities for ^{65}Zn were 41.7 ± 7.2 kBq/mg for uncoated ^{65}ZnO and 37.7 ± 5.0 kBq/mg for silica-coated ^{65}ZnO NPs.

Author Manuscript Author Manuscript Author Manuscript Author Manuscript

Preparation and characterization of uncoated ZnO and silica-coated ZnO nanoparticle suspensions

Uncoated and silica-coated ZnO NPs were dispersed using a protocol previously described (Cohen et al., 2013, Gass et al., 2013). The NPs were dispersed in deionized water at a concentration of 1 mg/ml and then sonicated at 242 J/ml sonication energy (20 min/ml at 0.2 watt power output). Deionized water (DI) was chosen to minimize the formation of reactive oxygen species and surface alterations on the nanoparticles due to components of physiological saline or other dispersant solutions. Samples were thoroughly mixed by vortexing immediately prior to injection. Dispersions of NPs were analyzed for hydrodynamic diameter (d_H), polydispersity index (PdI), and zeta potential (ζ) by dynamic light scattering (DLS) using a Zetasizer Nano-ZS (Malvern Instruments, Worcestershire, UK).

Animals

The protocols used in this study were approved by the Harvard Medical Area Animal Care and Use Committee. Nine-week-old male Wistar Han rats were purchased from Charles River Laboratories (Wilmington, MA, USA). Rats were housed in pairs in polysulfone cages and allowed to acclimate for 1 week before the studies were initiated. Rats were maintained on a 12-hour light/dark cycle. Food and water were provided *ad libitum*.

Pharmacokinetics of IV-injected neutron-activated uncoated ^{65}ZnO and silica-coated ^{65}ZnO nanoparticles

A total of thirty-four rats (mean wt., 286 ± 20 g) were used in this study. They were randomly assigned to uncoated ^{65}ZnO (n=17) or silica-coated ^{65}ZnO (n=17) NP groups. The first experiment was performed to determine the influence of amorphous silica coating on the vascular clearance kinetics of ^{65}Zn over a period of 120 minutes. Twelve rats per NP group were IV-injected via the penile vein with either NP suspension (1 mg/ml) immediately after sonication (1 mg/kg dose) as described above. Blood samples (0.25 – 0.35 ml) were collected via the tail vein at 1, 2, 5, 10, 20, 30 and 120 minutes post-injection. Blood samples were immediately placed in EDTA-coated collection tubes. All samples were centrifuged to separate plasma and blood cells. The packed red blood cells were washed in normal saline twice to remove any residual plasma and loosely associated ^{65}Zn from the RBCs. Separate plasma and RBC samples were placed in pre-weighed tubes for gamma counting. Sample weights were recorded. At 30 minutes and 2 hours post-injection, 7 and 5 rats were euthanized, respectively. Each rat was anesthetized and exsanguinated from the abdominal aorta. The lungs, brain, heart, spleen, kidneys, gastrointestinal tract, liver, and testes, and samples of skeletal muscle, bone marrow, skin, and femoral bone were collected and placed in pre-weighed tubes. Sample weights were recorded and radioactivity (1000–1225 KeV) measured in a WIZARD gamma counter (PerkinElmer, Inc., Waltham, MA, USA). Disintegrations per minute were calculated from the counts per minute and the counter efficiency. All radioactivity data were adjusted for physical decay over the entire observation period. Data were expressed as kBq/g and as a percentage of the administered dose retained in each organ. Total radioactivity in organs and tissues not measured in their entirety was computed using the following estimates of tissue percentage of total body

Author Manuscript Author Manuscript Author Manuscript Author Manuscript

weight: skeletal muscle, 40%; bone marrow, 3.2%; peripheral blood, 7%; skin, 19%; and bone, 6% (Brown et al., 1997, Schoeffner et al., 1999).

The remaining 10 rats were also IV-injected with the same NPs as described above (n=5 rats/NP). This was performed to determine the influence of amorphous silica coating on ZnO NPs on clearance of ^{65}Zn over a period of 7 days. Immediately after injection of NP suspension, each rat was placed in a metabolism cage. Twenty-four-hour fecal and urine samples were collected during the first 24 hours, and then at 2–3 and 6–7 days. At 7 days, rats were anesthetized and blood collected from the abdominal aorta. Sample collection and analyses were performed as described above. Fecal and urine samples were also analyzed for ^{65}Zn activities. Cumulative fecal and urine excretion kinetics were derived from these data.

Protein corona analysis of uncoated ZnO and silica-coated ZnO nanoparticles

Nanoparticles (1 mg/mL) were incubated in 4 mL rat plasma for 30 min at 37°C and then centrifuged for 10 min at 14,500 × g. The resulting pellet was washed in DI water three times. After the final washing step, the NP pellet with its 'hard corona' was suspended in 20 μL of DI water to which 10 μL of 4× Laemmli sample buffer was added. The sample was vortexed, and heated to 95°C for 7 min. After cooling to room temperature, 6 μL of mixed solution (57 μL Laemmli and 3 μL β mercaptoethanol (βME) was added to 18 μL of the sample. The samples were then loaded onto a gel and proteins were visualized by 1D SDS-PAGE in combination with Coomassie staining. Gel bands were excised and subjected to a modified in-gel trypsin digestion procedure (Shevchenko et al., 1996). Peptides were later extracted and then dried in a speed-vac (~1 hr). The samples were stored at 4°C until analysis. On the day of analysis the samples were reconstituted in 5 – 10 μL of HPLC solvent A (2.5% acetonitrile, 0.1% formic acid). A gradient was formed and peptides were eluted with increasing concentrations of solvent B (97.5% acetonitrile, 0.1% formic acid) (Peng and Gygi, 2001). Eluted peptides were subjected to electrospray ionization and then analyzed in an LTQ Orbitrap Velos Pro ion-trap mass spectrometer (Thermo Fisher Scientific, San Jose, CA, USA). Peptides were detected, isolated, and fragmented to produce a tandem mass spectrum of specific fragment ions for each peptide. Peptide sequences (and protein identities) were determined by matching protein databases with their acquired fragmentation pattern using Sequest software (ThermoFisher, San Jose, CA, USA) (Eng et al., 1994).

Statistical analyses

All tissue ^{65}Zn distribution data were analyzed using multivariate analysis of variance (MANOVA) followed by Bonferroni (Dunn) *post hoc* tests using SAS Statistical Analysis software (SAS Institute, Cary, NC, USA). Plasma clearance half-lives were calculated with a two-phase estimation by a biexponential model using R Program v. 3.1.0 (Jaki and Wolfsegger, 2011) (The R Foundation for Statistical Computing, Vienna, Austria)

Author Manuscript Author Manuscript Author Manuscript Author Manuscript

Results

Synthesis and characterization of uncoated ZnO and silica-coated ZnO NPs

As described earlier, uncoated and silica-coated ZnO NPs were synthesized using a flame spray pyrolysis technique (Demokritou et al., 2010, Sotiriou et al., 2014). The detailed physicochemical and morphological characterization of these NPs was reported earlier (Sotiriou et al., 2014, Gass et al., 2013). Briefly, the ZnO primary NPs had a rod-like shape with an aspect ratio of 2:1 to 8:1 (Figure 1). Flame-made nanoparticles typically exhibit a lognormal size distribution with geometric standard deviation σ_g = 1.45. To create the silica-coated ZnO nanorods, a nanothin (~ 4.6 ± 2.5 nm) amorphous silica layer encapsulated the ZnO core in flight, using an SiO_2 coating reactor (Gass et al., 2013) (Fig. 1B). The amorphous nature of the silica coating was verified by XRD and electron microscopy analyses. The physicochemical characterizations of the NPs are summarized in Table 1. The average crystal size of uncoated and silica-coated NPs were 29 and 28 nm, respectively. Their specific surface areas (SSA) were 41 m^2/g (uncoated) and 55 m^2/g (silica-coated). The lower density of silica compared to ZnO contributes to the higher SSA of the silica-coated ZnO than uncoated NPs.

The extent of the silica coating was assessed by X-ray photoelectron spectroscopy and photocatalytic experiments as described previously (Sotiriou et al., 2014). These data showed that less than 5% of ZnO NPs were uncoated, as some of the freshly formed core ZnO NPs may escape the coating process (Buesser and Pratsinis, 2011, Sotiriou et al., 2014).

After sonication at 242 J/ml, the NP suspensions had hydrodynamic diameters of 322 ± 1 nm (uncoated) and 460 ± 7 nm (silica-coated). Their zeta potential values were 30 ± 0.7 mV (uncoated) and −15.4 ± 1.3 mV (silica-coated). The zeta potentials were shown to differ over the pH range of 2.5–8.0 (Sotiriou et al., 2014), which includes the pH of blood and phagolysosomal compartments. After incubation in rat plasma and the formation of the protein corona, the hydrodynamic diameters of both ZnO NP types were significantly increased and the surface charge of uncoated ZnO was altered from positive to negative zeta potential (Table 1).

Effects of amorphous silica coating on ^{65}ZnO nanoparticle vascular clearance kinetics

Figure 2A shows the plasma ^{65}Zn levels as % of injected dose over 120 minutes. Silica-coated ^{65}ZnO NPs were more rapidly cleared from the plasma. The plasma clearance of both NPs was biphasic, with a rapid initial phase during the first 5 minutes ($t_{1/2}$: silica-coated ^{65}ZnO = < 1 min; ^{65}ZnO = 1.9 min) and a slower terminal phase ($t_{1/2}$: silica-coated ^{65}ZnO = 2.5; ^{65}ZnO = 38 min). Figure 2B shows the RBC-associated ^{65}Zn levels over time. The amount of ^{65}Zn in the plasma represents the amount of circulating material as yet uncleared from the circulation while the RBC-associated fraction of ^{65}Zn is either ions or NPs bound to or incorporated in the RBC. Silica-coated ^{65}ZnO NPs, cleared faster from the circulation, were immediately taken up in the liver, presumably by Kupffer cells, and their ^{65}Zn was also initially seen within RBCs as shown in Figure 2B. From 2 hours to 7 days (not shown), the RBC-associated ^{65}Zn from uncoated NPs increased to higher levels than those from coated ^{65}ZnO NPs.

Author Manuscript Author Manuscript Author Manuscript Author Manuscript

Effects of amorphous silica coating on tissue distributions of ^{65}Zn from ZnO nanoparticles

Figure 3 shows the tissue distribution of ^{65}Zn as % of injected ^{65}Zn dose at 30 min, 2 hours and 7 days post-injection. Figure 4 shows data for the liver, bone, skeletal muscle, skin and plasma. At all three time points, silica coating generally reduced ^{65}Zn retention in all organs except the liver, where ^{65}Zn levels from coated NPs were much higher especially at 30 min and 2 hours (Figure 4A). The silica coating also increased ^{65}Zn retention in the lungs but only at 30 minutes post-injection. By day 7, liver and plasma ^{65}Zn were significantly reduced in both NP groups (Figure 4A, 4E). Therefore, although the initial liver uptake was higher, ^{65}Zn from silica-coated NPs was cleared relatively faster than from uncoated NPs. ^{65}Zn from uncoated NPs accumulated in bone and skeletal muscle over time, while ^{65}Zn from silica-coated NPs accumulated in bone and skin (Figure 4B, 4C, 4D). The overall body ^{65}Zn clearance in both NP groups was similar (Figure 4F). We estimated the amounts of retained Zn in each tissue based on the measured ^{65}Zn/g and specific activity of ^{65}Zn. Table 2 shows the zinc concentration in each tissue at 30 min, 2 hours and 7 days post-injection. The data shows that in almost all tissues except the liver, the silica coating caused significant reductions in zinc retention. Urinary excretion of ^{65}Zn was much lower than fecal excretion. Urinary and fecal excretion of ^{65}Zn did not differ between uncoated and silica-coated ^{65}ZnO NPs (Figure 5).

Protein corona analysis of uncoated ZnO and silica-coated ZnO nanoparticles

Figure 6 shows the SDS-PAGE gel electrophoresis of eluted proteins from the washed ZnO NPs after a 30 min incubation in rat plasma at 37°C. Representative SDS gel and protein quantification are shown in Figure 6A and 6B, respectively. Plasma protein adsorption, particularly albumin, transferrin, A1 inhibitor 3, α-2-hs-glycoprotein, α-1 antitrypsin, and apoprotein E was higher in the corona of silica-coated (139 μg/mg NPs) than uncoated ZnO NPs (80 μg/mg NPs).

Discussion

Developing strategies to alter the surface of NPs without changing their core properties is an active area of research. Coating NPs with amorphous silica is a possible strategy to enhance their colloidal stability and biocompatibility for a variety of medical applications (Alwi et al., 2012, Jana et al., 2007). Surface characteristics of NPs, such as chemical and molecular structure, influence their pharmacokinetic behavior (Buzea et al., 2007, Sund et al., 2011). Intrinsic properties of NPs including surface chemistry, charge and size influence the adsorption of proteins, lipids and other biomolecules in the blood leading to the formation of a particle corona. This in turn will affect the cellular uptake, localization, biodistribution, and host responses to NPs (Cedervall et al., 2007, Lynch et al., 2009, Monopoli et al., 2012). We found that the coating of ZnO NPs with amorphous silica altered the protein corona composition when incubated in rat plasma, increased their agglomerate sizes of both NPs, and altered the zeta potential of the uncoated ZnO from positive to negative. Our results also demonstrate that uncoated ZnO and silica-coated ZnO NPs were both cleared rapidly from the circulation within 120 minutes after IV-injection. However, silica-coated ZnO NPs were cleared from plasma much faster than uncoated ZnO NPs, and become more associated with RBCs. This implies that silica coating enhances NP interaction with RBCs. A previous study

Author Manuscript Author Manuscript Author Manuscript Author Manuscript

has shown that silanols and siloxane groups in amorphous silica interact with specific epitopes on the RBC membrane and cause hemolysis in vitro (Pavan et al., 2014). We did not observe hemolysis in vivo perhaps due to a rapid formation of the protein corona on NPs soon after injection or an absence of organics on silica surfaces that are seen during high-temperature synthesis. Alternatively, the higher levels of ^{65}Zn in the RBCs of silica-coated NP-injected rats may have resulted from the enhanced uptake of NPs by Kupffer cells and other macrophages, followed by Zn ion release and adsorption into the RBCs.

We propose that varying corona composition influences the differences in vascular kinetics between uncoated and silica-coated ZnO NPs. A previous study showed adsorption of numerous plasma and brain homogenate proteins with different sized and surface charged ZnO NPs (Shim et al., 2014). Similarly, it was reported that adsorbed proteins on gold nanoparticles decrease with increasing AuNP sizes after a 24-hour incubation in mouse serum in vitro (Schaffler et al., 2013). We found that binding of plasma proteins to ZnO surface was also altered by the silica coating. Notably, bound albumin, transferrin, A1 inhibitor 3, α-2-hs-glycoprotein, α-1 antitrypsin, and apoprotein E were relatively higher in silica-coated ZnO. These proteins were similar to those described on gold nanoparticles (Schaffler et al., 2013).

A recent study showed that albumin-coated liposomes were taken up more efficiently than uncoated liposomes by murine macrophages (Vuarchey et al., 2011). However, it has been reported that conjugation of radiolabeled (^{198}Au) gold nanoparticles with human serum albumin or apolipoprotein E prior to IV injection in mice significantly reduced liver retention of 15 nm but not of 80 nm NPs (Schaffler et al., 2014). In the present study, while the silica coating of ZnO NPs enhanced albumin adsorption, it led to an increased initial retention in the liver (65.7 vs. 29.1%) and spleen (1.2 vs. 0.7%) measured at 30 minutes. The role of the other adsorbed proteins in NP liver uptake is unknown. We also found that the clearance of ^{65}Zn from silica-coated NPs was faster such that by day 7, the liver retention was similar (4% - uncoated; 4.6% - silica-coated). This may be due to the influence of silica coating on Kupffer cell processing and dissolution of ZnO. We hypothesized that silica coating would reduce the dissolution of ZnO NPs in the Kupffer cells and this in turn would contribute to a higher retention of Zn in the liver. But what we found was only a transient increase in liver retention of silica-coated ZnO NPs. Although the silica coating initially enhanced the liver uptake, by day 7, the retained ^{65}Zn was not different from the uncoated ZnO NP group. This may be due to the fast dissolution of ZnO NPs within Kupffer cells. Regardless of difference in the initial uptake, the hepatic clearance of Zn from both uncoated and silica-coated NPs was similar. The rapid sequestration of coated ZnO NPs in the liver reduced the circulating NPs available for uptake by other organs (Figure 2). Thus, ^{65}Zn concentrations in tissues other than the liver were significantly lower (Table 2).

Conclusions

We conclude that coating ^{65}ZnO NPs with a nanothin layer of amorphous silica alters the nanoparticle interaction with plasma proteins as well as their subsequent fate after intravenous injection. The silica coating elicits the formation of a denser protein corona, more rapid clearance from the circulation, and a higher uptake in the liver. Additionally, it

Author Manuscript Author Manuscript Author Manuscript Author Manuscript

also reduced tissue retention of ^{65}Zn in all other organs examined. Our data indicate that surface modifications of ZnO NPs, such as coating with amorphous silica, may alter their biokinetics, toxicity, and thus potential medical applications.

Acknowledgments

This study was supported by NSF (1235806) and NIEHS grant (ES 0000002). KMM received a Graduate Research Fellowship from the National Science Foundation (DGE-1144152). The authors gratefully acknowledge the financial support of BASF. We thank Melissa Curran for editorial assistance.

References

ALARIFI S, ALI D, ALKAHTANI S, VERMA A, AHAMED M, AHMED M, ALHADLAQ HA. Induction of oxidative stress, DNA damage, and apoptosis in a malignant human skin melanoma cell line after exposure to zinc oxide nanoparticles. Int J Nanomed. 2013; 8:983–93.

ALWI R, TELENKOV S, MANDELIS A, LESHUK T, GU F, OLADEPO S, MICHAELIAN K. Silica-coated super paramagnetic iron oxide nanoparticles (SPION) as biocompatible contrast agent in biomedical photoacoustics. Biomed Opt Express. 2012; 3:2500–9. [PubMed: 23082291]

BAEK M, CHUNG HE, YU J, LEE JA, KIM TH, OH JM, LEE WJ, PAEK SM, LEE JK, JEONG J, CHOY JH, CHOI SJ. Pharmacokinetics, tissue distribution, and excretion of zinc oxide nanoparticles. Int J Nanomed. 2012; 7:3081–97.

BAEK M, KIM MK, CHO HJ, LEE JA, YU J, CHUNG HE, CHOI SJ. Factors influencing the cytotoxicity of zinc oxide nanoparticles: particle size and surface charge. J Physics: Conf Series. 2011:304.

BROWN RP, DELP MD, LINDSTEDT SL, RHOMBERG LR, BELILES RP. Physiological parameter values for physiologically based pharmacokinetic models. Toxicol Ind Health. 1997; 13:407–84. [PubMed: 9249929]

BUESSER B, PRATSINIS SE. Design of Gas-phase Synthesis of Core-Shell Particles by Computational Fluid - Aerosol Dynamics. AIChE J. 2011; 57:3132–3142. [PubMed: 23729817]

BUZEA C, PACHECO, ROBBIE K. Nanomaterials and nanoparticles: sources and toxicity. Biointerphases. 2007; 2:MR17–71. [PubMed: 20419892]

CEDERVALL T, LYNCH I, LINDMAN S, BERGGARD T, THULIN E, NILSSON H, DAWSON KA, LINSE S. Understanding the nanoparticle-protein corona using methods to quantify exchange rates and affinities of proteins for nanoparticles. Proc Natl Acad Sci USA. 2007; 104:2050–5. [PubMed: 17267609]

CHEN JK, SHIH MH, PEIR JJ, LIU CH, CHOU FI, LAI WH, CHANG LW, LIN P, WANG MY, YANG MH, YANG CS. The use of radioactive zinc oxide nanoparticles in determination of their tissue concentrations following intravenous administration in mice. The Analyst. 2010; 135:1742–6. [PubMed: 20505857]

CHOI HS, LIU W, MISRA P, TANAKA E, ZIMMER JP, ITTY IPE B, BAWENDI MG, FRANGIONI JV. Renal clearance of quantum dots. Nat Biotechnol. 2007; 25:1165–70. [PubMed: 17891134]

CHOI SJ, CHOY JH. Biokinetics of zinc oxide nanoparticles: toxicokinetics, biological fates, and protein interaction. Int J Nanomed. 2014; 9(Suppl 2):261–9.

COHEN J, DELOID G, PYRGIOTAKIS G, DEMOKRITOU P. Interactions of engineered nanomaterials in physiological media and implications for in vitro dosimetry. Nanotoxicology. 2013; 7:417–31. [PubMed: 22393878]

DE BERARDIS B, CIVITELLI G, CONDELLO M, LISTA P, POZZI R, ARANCIA G, MESCHINI S. Exposure to ZnO nanoparticles induces oxidative stress and cytotoxicity in human colon carcinoma cells. Toxicol Appl Pharmacol. 2010

DEMOKRITOU P, BUCHEL R, MOLINA RM, DELOID GM, BRAIN JD, PRATSINIS SE. Development and characterization of a Versatile Engineered Nanomaterial Generation System (VENGES) suitable for toxicological studies. Inhal Toxicol. 2010; 22(Suppl 2):107–16. [PubMed: 20701428]

Author Manuscript Author Manuscript Author Manuscript Author Manuscript

DEMOKRITOU P, GASS S, PYRGIOTAKIS G, COHEN JM, GOLDSMITH W, MCKINNEY W, FRAZER D, MA J, SCHWEGLER-BERRY D, BRAIN J, CASTRANOVA V. An in vivo and in vitro toxicological characterisation of realistic nanoscale CeO_2 inhalation exposures. Nanotoxicology. 2013; 7:1338–1350. [PubMed: 23061914]

DJURISIC AB, LEUNG YH. Optical properties of ZnO nanostructures. Small. 2006; 2:944–61. [PubMed: 17193149]

ENG JK, MCCORMACK AL, YATES JR. An approach to correlate tandem mass spectral data of peptides with amino acid sequences in a protein database. J Am Soc Mass Spectrom. 1994; 5:976–89. [PubMed: 24226387]

GASS S, COHEN JM, PYRGIOTAKIS G, SOTIRIOU GA, PRATSINIS SE, DEMOKRITOU P. A Safer Formulation Concept for Flame-Generated Engineered Nanomaterials. ACS Sustain Chem Eng. 2013; 1:843–857. [PubMed: 23961338]

JAKI T, WOLFSEGGER MJ. Estimation of pharmacokinetic parameters with the R package PK. Pharm Stat. 2011; 10:288–294.

JANA NR, YU HH, ALI EM, ZHENG Y, YING JY. Controlled photostability of luminescent nanocrystalline ZnO solution for selective detection of aldehydes. Chem Commun (Camb). 2007:1406–8. [PubMed: 17389974]

KONDURU NV, JIMENEZ RJ, SWAMI A, FRIEND S, CASTRANOVA V, DEMOKRITOU P, BRAIN JD, MOLINA RM. Silica coating influences the corona and biokinetics of cerium oxide nanoparticles. Part Fibre Toxicol. 2015; 12:31. [PubMed: 26458946]

KONDURU NV, MURDAUGH KM, SOTIRIOU GA, DONAGHEY TC, DEMOKRITOU P, BRAIN JD, MOLINA RM. Bioavailability, distribution and clearance of tracheally-instilled and gavaged uncoated or silica-coated zinc oxide nanoparticles. Part Fibre Toxicol. 2014; 11:44. [PubMed: 25183210]

KREYLING WG, FERTSCH-GAPP S, SCHAFFLER M, JOHNSTON BD, HABERL N, PFEIFFER C, DIENDORF J, SCHLEH C, HIRN S, SEMMLER-BEHNKE M, EPPLE M, PARAK WJ. In vitro and in vivo interactions of selected nanoparticles with rodent serum proteins and their consequences in biokinetics. Beilstein J Nanotechnol. 2014; 5:1699–711. [PubMed: 25383281]

KREYLING WG, GODLESKI JJ, KARIYA ST, ROSE RM, BRAIN JD. In vitro dissolution of uniform cobalt oxide particles by human and canine alveolar macrophages. Am J Respir Cell Mol Biol. 1990; 2:413–22. [PubMed: 2340182]

LYNCH I, SALVATI A, DAWSON KA. Protein-nanoparticle interactions: What does the cell see? Nature Nanotechnol. 2009; 4:546–7. [PubMed: 19734922]

MOGHIMI SM, HUNTER AC, ANDRESEN TL. Factors controlling nanoparticle pharmacokinetics: an integrated analysis and perspective. Annu Rev Pharmacol Toxicol. 2012; 52:481–503. [PubMed: 22035254]

MONOPOLI MP, ABERG C, SALVATI A, DAWSON KA. Biomolecular coronas provide the biological identity of nanosized materials. Nature Nanotechnol. 2012; 7:779–86. [PubMed: 23212421]

NOHYNEK GJ, DUFOUR EK, ROBERTS MS. Nanotechnology, cosmetics and the skin: is there a health risk? Skin Pharmacol Physiol. 2008; 21:136–49. [PubMed: 18523411]

NOHYNEK GJ, LADEMANN J, RIBAUD C, ROBERTS MS. Grey goo on the skin? Nanotechnology, cosmetic and sunscreen safety. Crit Rev Toxicol. 2007; 37:251–77. [PubMed: 17453934]

PAEK HJ, LEE YJ, CHUNG HE, YOO NH, LEE JA, KIM MK, LEE JK, JEONG J, CHOI SJ. Modulation of the pharmacokinetics of zinc oxide nanoparticles and their fates in vivo. Nanoscale. 2013; 5:11416–27. [PubMed: 23912904]

PAVAN C, RABOLLI V, TOMATIS M, FUBINI B, LISON D. Why does the hemolytic activity of silica predict its pro-inflammatory activity? Part Fibre Toxicol. 2014; 11:76. [PubMed: 25522817]

PENG J, GYGI SP. Proteomics: the move to mixtures. J Mass Spectrom. 2001; 36:1083–91. [PubMed: 11747101]

SCHAFFLER M, SEMMLER-BEHNKE M, SARIOGLU H, TAKENAKA S, WENK A, SCHLEH C, HAUCK SM, JOHNSTON BD, KREYLING WG. Serum protein identification and quantification of the corona of 5, 15 and 80 nm gold nanoparticles. Nanotechnology. 2013; 24:265103. [PubMed: 23735821]

Author Manuscript Author Manuscript Author Manuscript Author Manuscript

SCHAFFLER M, SOUSA F, WENK A, SITIA L, HIRN S, SCHLEH C, HABERL N, VIOLATTO M, CANOVI M, ANDREOZZI P, SALMONA M, BIGINI P, KREYLING WG, KROL S. Blood protein coating of gold nanoparticles as potential tool for organ targeting. Biomaterials. 2014; 35:3455–66. [PubMed: 24461938]

SCHOEFFNER DJ, WARREN DA, MURALIDARA S, BRUCKNER JV, SIMMONS JE. Organ weights and fat volume in rats as a function of strain and age. J Toxicol Environ Health A. 1999; 56:449–62. [PubMed: 10201633]

SHEVCHENKO A, WILM M, VORM O, MANN M. Mass spectrometric sequencing of proteins silver-stained polyacrylamide gels. Anal Chem. 1996; 68:850–8. [PubMed: 8779443]

SHIM KH, HULME J, MAENG EH, KIM MK, AN SS. Analysis of zinc oxide nanoparticles binding proteins in rat blood and brain homogenate. Int J Nanomed. 2014; 9(Suppl 2):217–24.

SOTIRIOU GA, WATSON C, MURDAUGH KM, DARRAH TH, PYRGIOTAKIS G, ELDER A, BRAIN JD, DEMOKRITOU P. Engineering safer-by-design, transparent, silica-coated ZnO nanorods with reduced DNA damage potential. Environ Sci:Nano. 2014; 1:144–153. [PubMed: 24955241]

SU YK, PENG SM, JI LW, WU CZ, CHENG WB, LIU CH. Ultraviolet ZnO nanorod photosensors. Langmuir. 2010; 26:603–6. [PubMed: 19894681]

SUND J, ALENIUS H, VIPPOLA M, SAVOLAINEN K, PUUSTINEN A. Proteomic characterization of engineered nanomaterial-protein interactions in relation to surface reactivity. ACS Nano. 2011; 5:4300–9. [PubMed: 21528863]

VUARCHEY C, KUMAR S, RS. Albumin coated liposomes: a novel platform for macrophage specific drug delivery. Nanotechnol Dev. 2011; 1:5–10.

WARHEIT DB, SAYES CM, REED KL. Nanoscale and fine zinc oxide particles: can in vitro assays accurately forecast lung hazards following inhalation exposures? Environ Sci Technol. 2009; 43:7939–45. [PubMed: 19921917]

XIA T, KOVOCHICH M, LIONG M, MADLER L, GILBERT B, SHI H, YEH JI, ZINK JI, NEL AE. Comparison of the mechanism of toxicity of zinc oxide and cerium oxide nanoparticles based on dissolution and oxidative stress properties. ACS Nano. 2008; 2:2121–34. [PubMed: 19206459]

YEH TK, CHEN JK, LIN CH, YANG MH, YANG CS, CHOU FI, PEIR JJ, WANG MY, CHANG WH, TSAI MH, TSAI HT, LIN P. Kinetics and tissue distribution of neutron-activated zinc oxide nanoparticles and zinc nitrate in mice: effects of size and particulate nature. Nanotechnology. 2012; 23:085102. [PubMed: 22293282]

Author Manuscript Author Manuscript Author Manuscript Author Manuscript

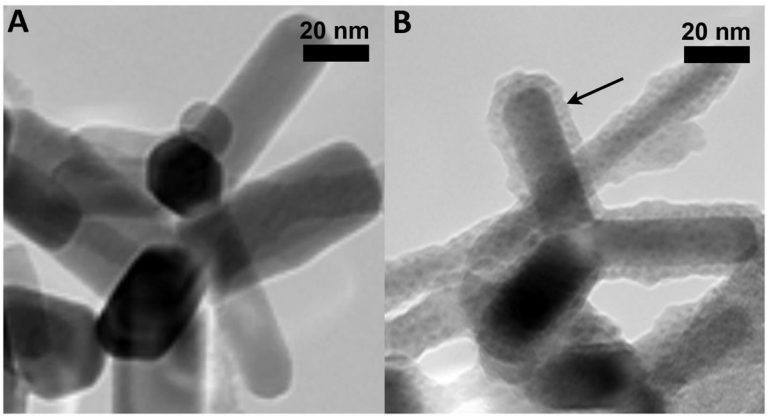

Figure 1.

Transmission electron micrograph of uncoated ZnO (A) and silica-coated ZnO (B) NPs. (Note: arrow points to the thin silica coating of approximately 5 nm in B). In both cases, the ZnO NPs have a rod-like shape with an aspect ratio of 2:1 to 8:1 (Sotiriou et al., 2014).

Author Manuscript Author Manuscript Author Manuscript Author Manuscript

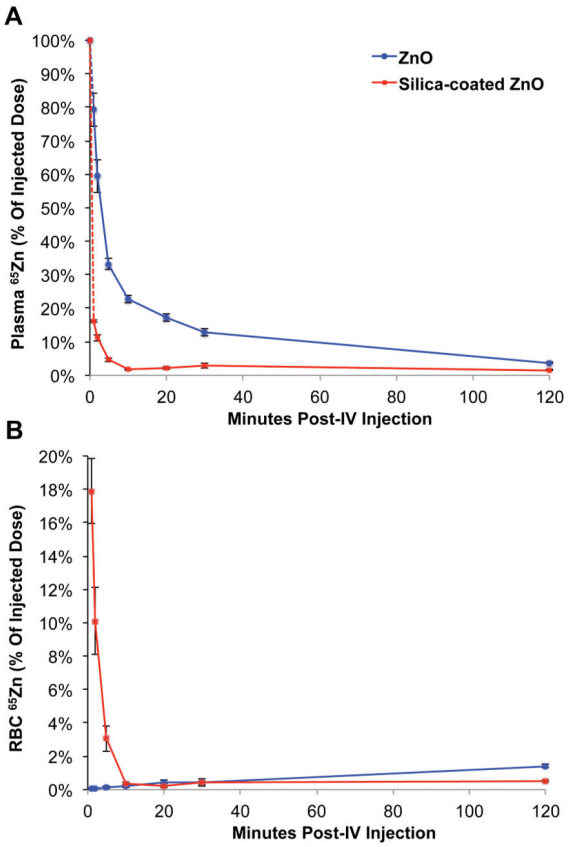

Figure 2.

Vascular kinetics of IV-injected uncoated ^{65}ZnO and silica-coated ^{65}ZnO nanoparticles **A.** Plasma kinetics of IV-injected uncoated ^{65}ZnO and silica-coated ^{65}ZnO nanoparticles. **B.** Interaction of IV-injected uncoated ^{65}ZnO and silica-coated ^{65}ZnO nanoparticles with circulating red blood cells. Data are mean ± SE, n=5–7 rats/group.

Author Manuscript Author Manuscript Author Manuscript Author Manuscript

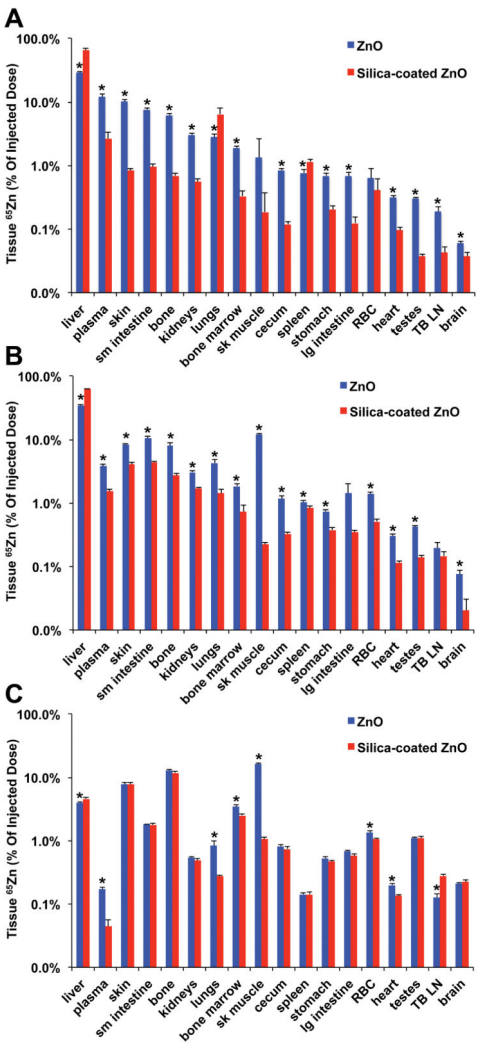

Figure 3.

Tissue distribution of uncoated ^{65}Zn post-IV- injection of uncoated ^{65}ZnO and silica-coated ^{65}ZnO nanoparticles. **A.** 30 minutes **B**. 2 hours. **C.** 7 days post-injection. The y-axes are in logarithmic scale. Data are mean ± SE, n=5–7 rats/group. * MANOVA, $P < 0.05$. Differences between uncoated and silica-coated ^{65}ZnO were significant in all tissues except RBC and skeletal muscle at 30 minutes (**A**), TB LN and large intestine at 2 hours (**B**). Significant differences in the liver, plasma, lungs, bone marrow, skeletal muscle, RBC, heart and tracheobronchial lymph nodes were observed at 7 days (**C**).

Author Manuscript Author Manuscript Author Manuscript Author Manuscript

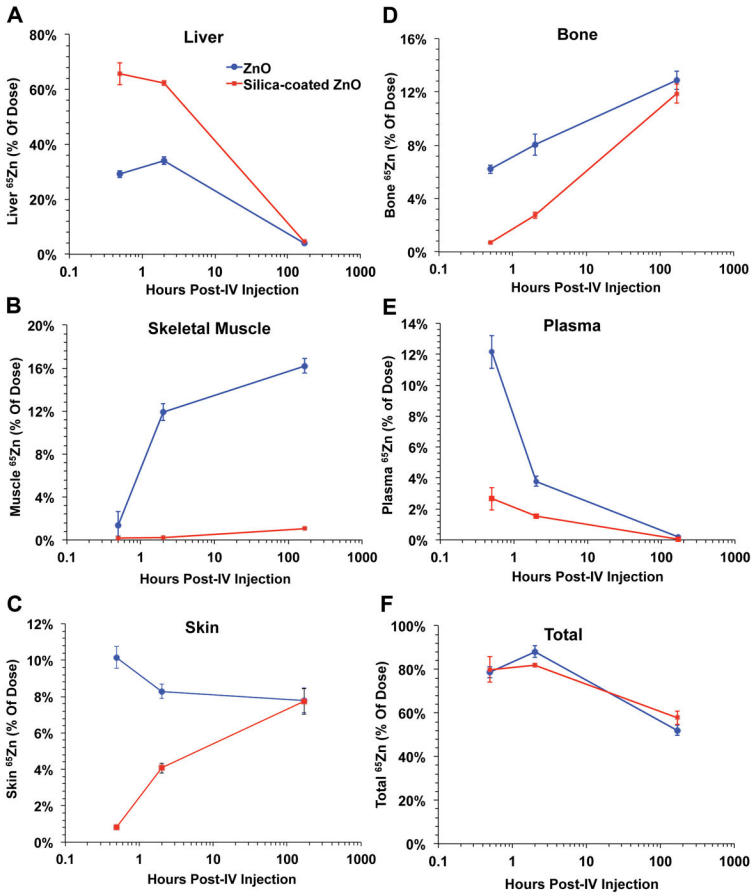

Figure 4.

Selected organ retention of ^{65}Zn over time. Liver (**A**), skeletal muscle (**B**), bone (**C**), and total body (**D**) retention of ^{65}Zn over 7 days post-IV- injection of uncoated or silica-coated ^{65}ZnO nanoparticles. The x-axes are in logarithmic scale. Data are mean ± SE, n=5–7 rats/group.

Author Manuscript Author Manuscript Author Manuscript Author Manuscript

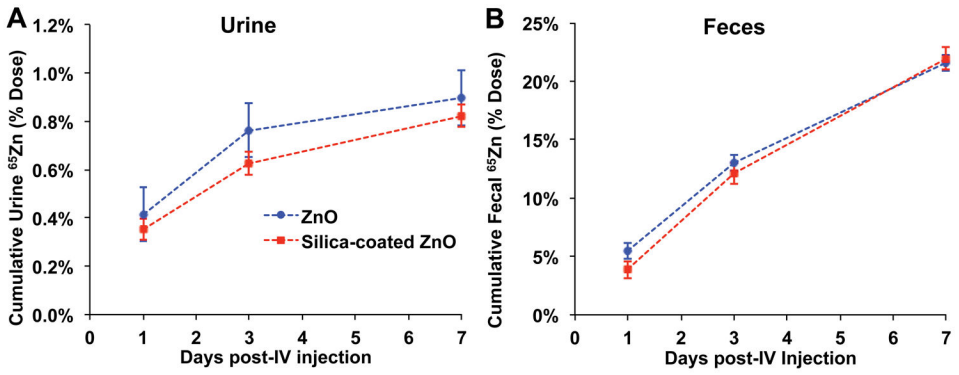

Figure 5.

Excretion of ^{65}Zn post-injection of uncoated ^{65}ZnO and silica-coated ^{65}ZnO nanoparticles. **A.** Urinary excretion. **B.** Fecal excretion. Data are mean ± SE, n=5 rats/group. No differences in cumulative urine and fecal excretion between uncoated and silica-coated ^{65}ZnO nanoparticles were observed.

Author Manuscript Author Manuscript Author Manuscript Author Manuscript

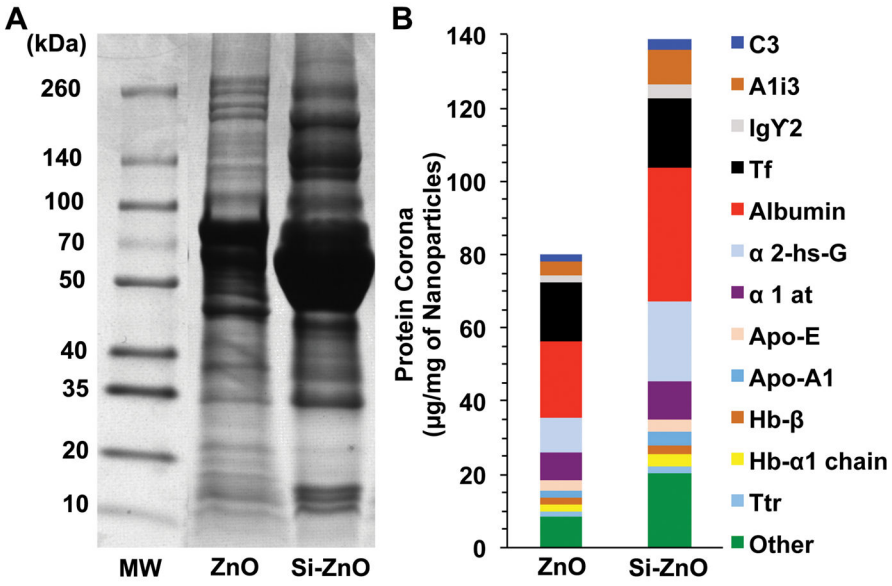

Figure 6.

Analysis of ZnO NP-bound rat plasma proteins by 1D gel electrophoresis (**A**) and Mass Spectrometry (**B**). The molecular weights (kDa) of reference proteins are shown in lane MW. (**B**) Twelve proteins identified by LC-MS and quantified based on densitometry of gel bands in **A**.

Author Manuscript

Author Manuscript

Author Manuscript

Author Manuscript

Table 1

Physicochemical characterization of nanoparticles.

	Uncoated ZnO	Silica-coated ZnO	Uncoated ZnO with corona	Silica-coated ZnO with corona
SSA (m^2/g) *	41.0	55.0	N.A.	N.A.
D_{xrd} (nm) *	29.0	28.0	N.A.	N.A.
D_H (nm)	322 ± 1	460 ± 7	2039 ± 163	2119 ± 64
ζ(mv)	30.1 ± 0.7	−15.4 ± 1.3	−27.2 ± 2.0	−19.6 ± 2.8

SSA – specific surface area

D_{xrd} – primary particle size based on X-ray diffraction

D_H – hydrodynamic diameter

ζ - zeta potential

N.A. – not applicable.

* SSA and D_{xrd} measurement for uncoated and silica-coated ZnO NPs were previously reported (Sotiriou et al., 2014)

Author Manuscript Author Manuscript Author Manuscript Author Manuscript

Nanotoxicology. Author manuscript; available in PMC 2017 August 01.

Table 2

Zinc concentration in tissues post-IV injection of uncoated ^{65}ZnO and silica-coated ^{65}ZnO.

	30 Minutes n = 7		2 Hours n = 5		7 Days n = 5	
Tissue	**Uncoated ZnO**	**Silica-coated ZnO**	**Uncoated ZnO**	**Silica-coated ZnO**	**Uncoated ZnO**	**Silica-coated ZnO**
Liver	8.30 ± 0.35	15.76 ± 1.13#	9.76 ± 0.54	11.15 ± 0.31#	1.14 ± 0.04*	0.80 ± 0.03
Lungs	6.30 ± 0.60	10.54 ± 1.83#	9.91 ± 2.38*	2.08 ± 0.31	1.77 ± 0.35*	0.33 ± 0.02
Kidneys	4.55 ± 0.33*	0.63 ± 0.03	4.15 ± 0.32*	1.52 ± 0.08	0.68 ± 0.02*	0.37 ± 0.02
Spleen	3.85 ± 0.70	4.92 ± 0.48	5.20 ± 0.28*	2.69 ± 0.20	0.71 ± 0.02*	0.40 ± 0.01
Plasma	3.04 ± 0.28*	0.39 ± 0.07	0.92 ± 0.06*	0.25 ± 0.01	0.04 ± 0.003*	0.01 ± 0.002
SI	2.33 ± 0.18*	0.24 ± 0.01	3.51 ± 0.29*	0.85 ± 0.04	0.55 ± 0.01*	0.31 ± 0.02
Heart	1.17 ± 0.07*	0.25 ± 0.01	1.02 ± 0.09*	0.26 ± 0.01	0.61 ± 0.01*	0.27 ± 0.02
Bone	1.04 ± 0.08*	0.09 ± 0.01	1.26 ± 0.12*	0.28 ± 0.02	1.94 ± 0.09*	1.11 ± 0.06
TB LN	0.92 ± 0.14*	0.16 ± 0.03	0.98 ± 0.07*	0.21 ± 0.04	0.78 ± 0.16*	0.32 ± 0.02
LI	0.84 ± 0.11*	0.09 ± 0.02	1.09 ± 0.39*	0.19 ± 0.04	0.47 ± 0.02*	0.29 ± 0.03
BM	0.61 ± 0.06*	0.08 ± 0.01	0.55 ± 0.06*	0.14 ± 0.04	0.97 ± 0.07*	0.44 ± 0.03
Skin	0.54 ± 0.06*	0.03 ± 0.002	0.41 ± 0.02*	0.13 ± 0.01	0.37 ± 0.03*	0.23 ± 0.02
Stomach	0.45 ± 0.08*	0.11 ± 0.02	0.51 ± 0.04*	0.23 ± 0.04	0.52 ± 0.06*	0.20 ± 0.03
Cecum	0.35 ± 0.02*	0.04 ± 0.003	0.53 ± 0.05*	0.10 ± 0.01	0.32 ± 0.02*	0.16 ± 0.01
SM	0.31 ± 0.03*	0.03 ± 0.01	0.28 ± 0.02*	0.06 ± 0.004	0.37 ± 0.01*	0.21 ± 0.01
Testes	0.27 ± 0.02*	0.03 ± 0.002	0.33 ± 0.02*	0.07 ± 0.01	0.89 ± 0.02*	0.49 ± 0.01
RBC	0.16 ± 0.04	0.09 ± 0.04	0.42 ± 0.04*	0.10 ± 0.01	0.37 ± 0.02*	0.18 ± 0.01
Brain	0.13 ± 0.01*	0.07 ± 0.02	0.13 ± 0.01*	0.02 ± 0.01	0.36 ± 0.01*	0.19 ± 0.01

Data are μg Zn/g tissue ± SE, n = 5–7 rats per group.

Each tissue zinc concentration was calculated based on the reciprocal of specific activity of NP (μg Zn/^{65}Zn) and measured tissue ^{65}Zn/g.

Formula: μg Zn/g tissue = μg Zn/^{65}Zn$_{(NP)}$ × ^{65}Zn/g$_{(tissue)}$

Data for silica-coated ZnO were adjusted to the Zn content of uncoated ZnO NPs.

Author Manuscript Author Manuscript Author Manuscript Author Manuscript

RBC=red blood cells, TB LN=tracheobronchial lymph nodes, BM=bone marrow, SM=skeletal muscle, SI=small intestine, LI=large intestine

*$P < 0.05$, MANOVA, uncoated ^{65}ZnO > silica-coated ^{65}ZnO

#$P < 0.05$, MANOVA, silica-coated ^{65}ZnO > uncoated ^{65}ZnO